ELSEVIER

Journal of Volcanology and Geothermal Research 120 (2002) 1–23

Journal of volcanology and geothermal research

www.elsevier.com/locate/jvolgeores

The evolution of bubble size distributions in volcanic eruptions

J.D. Blower [a], J.P. Keating [b], H.M. Mader [a,*], J.C. Phillips [a]

[a] *Department of Earth Sciences, University of Bristol, Bristol BS8 1RJ, UK*
[b] *School of Mathematics, University of Bristol, Bristol BS8 1TW, UK*

Received 3 December 2001; accepted 10 July 2002

Abstract

We review observations of bubble size distributions (BSDs) generated during explosive volcanic eruptions and laboratory explosions, as inferred from vesicle size distributions found in the end products. Unimodal, polymodal, exponential and power law BSDs are common, even in the absence of coalescence, and both power law and exponential distributions have been generated in the same eruption. To date theoretical models have proposed incompatible mechanisms for producing the various distributions. We here present a unifying mechanism. Data from our laboratory analogue experiments suggest that power law distributions are associated with highly non-equilibrium degassing. A numerical model is developed in which bubbles nucleate repeatedly and grow in the spaces between those of previous generations, where, in a non-equilibrium degassing scenario, the volatile concentration remains high. This process causes the BSD to evolve from unimodal, through exponential, into a power law. The exponent of the power law is a measure of the number of nucleation events, or the duration of the nucleation period compared with the timescale of bubble growth. The mathematical inevitability of the evolution from unimodal (Poissonian) to power law is discussed. The findings may resolve the apparent contradiction between the equilibrium degassing conduit flow models and the non-equilibrium degassing conditions derived from bubble growth models of explosive volcanic eruptions. The process of ongoing nucleation is the mechanism whereby the volcanic system maintains near-equilibrium in the case of rapid depressurisation and slow volatile diffusion.

1. Introduction

The inaccessibility of the interior of volcanic systems means that the dynamics of degassing cannot be directly observed in situ. Processes of bubble nucleation and growth must be inferred from secondary sources such as theoretical studies, laboratory investigations and textural examination of volcanic deposits. Over the last two decades the detailed analysis of the structure of volcanic rocks such as pumice, scoria and lava has become a standard tool in the deduction of eruption parameters. One of the most common textural parameters measured is the vesicle size distribution (VSD) of the solid rock, which is used to infer the bubble size distribution (BSD) generated during the liquid process of magma vesiculation. In this paper we are interested specifi-

* Corresponding author.
E-mail addresses: jon.blower@tessella.co.uk (J.D. Blower), j.p.keating@bristol.ac.uk (J.P. Keating), h.m.mader@bristol.ac.uk (H.M. Mader), j.c.phillips@bristol.ac.uk (J.C. Phillips).

0377-0273/02/$ – see front matter
PII: S0377-0273(02)00404-3

cally in the evolution of the BSD. (Wherever the term BSD is used in connection with solid samples, we are referring to the distribution of bubbles that resulted in the observed VSD.)

A number of theoretical models have been developed linking the BSD with eruption parameters such as the nucleation and growth rates of bubbles, the extent of bubble coalescence, magma ascent rate and volatile supersaturation. In 2. Background we summarise these methods and the data to which they have been applied. We then describe the results of a new study which incorporates laboratory analogue experiments, numerical modelling and observations of volcanic rocks. This new study reveals that exponential and power law BSDs, both commonly observed in volcanic rocks, may be generated by the same process of continuous bubble nucleation and growth. These findings may resolve the apparent contradiction between equilibrium conduit flow models and the non-equilibrium conditions derived from bubble growth models of explosive volcanic eruptions.

2. Background

Unimodal, polymodal, exponential and power law (fractal) BSDs have all been observed in natural magmatic rocks. The different distributions have hitherto been explained separately on the basis of fundamentally different physical processes. We use the symbol $N(R)$ to represent the number density function of the BSD; that is, $N(R)\mathrm{d}R$ is the number of bubbles with radii between R and $R+\mathrm{d}R$.

2.1. Unimodal and polymodal BSDs

Distributions containing one or more discrete peaks are reported by numerous workers (see e.g. Sparks and Brazier, 1982; Whitham and Sparks, 1986; Orsi et al., 1992). It is usually inferred that the different peaks arise from a corresponding number of temporally well-separated events. For example, the BSDs presented by Sparks and Brazier (1982) show three discrete peaks. The authors interpret the coarsest peak as originating from nucleation in the magma chamber prior to eruption. The peak at intermediate bubble size is attributed to nucleation during an eruption. The fine peak is not a separate bubble population but is due to apertures between vesicles (Whitham and Sparks, 1986). Similarly, the data of Orsi et al. (1992) show two peaks: one due to syn-eruptive nucleation and another attributed to subsequent bubble coalescence.

2.2. Exponential BSDs

Exponential BSDs are usually explained using a model based on the theory of Marsh (1988) for crystal size distributions. This approach assumes a steady state system in which the BSD does not change with time. A conservation law for the balance of bubbles growing into and out of a size class, given a constant growth rate G, produces an exponential distribution of the form:

$$N(R) = N_0 \exp\left(-\frac{R}{G\tau}\right) \quad (1)$$

where N_0 is the nucleation density ($N(R) = N_0$ for $R = 0$) and τ is the timescale available for bubble growth. The strength of this model lies largely in its convenience; eruption parameters may be calculated very simply from the BSD (Fig. 1). Note that in this case $G\tau$ represents a natural length scale for the bubble size.

The Marsh (1988) model has been applied in several studies (Sarda and Graham, 1990; Mangan et al., 1993; Klug and Cashman, 1994; Mangan and Cashman, 1996; Burnard, 1999). Of particular interest here is the study of Mangan and Cashman (1996) who examine samples of basaltic scoria from fire-fountaining episodes of Kilauea. They calculate nucleation rates of $\sim 2\times10^4$ cm^{-3} s^{-1}, much greater than the nucleation rate of 35.9 cm^{-3} s^{-1} estimated for effusive lava-flow activity (Mangan et al., 1993). This 'runaway' nucleation is interpreted as being due to the development of a high supersaturation before nucleation, consistent with the more explosive behaviour of the eruption.

The limitations of Marsh's model lie in the assumptions of steady state behaviour and constant bubble nucleation and growth rates. There is no

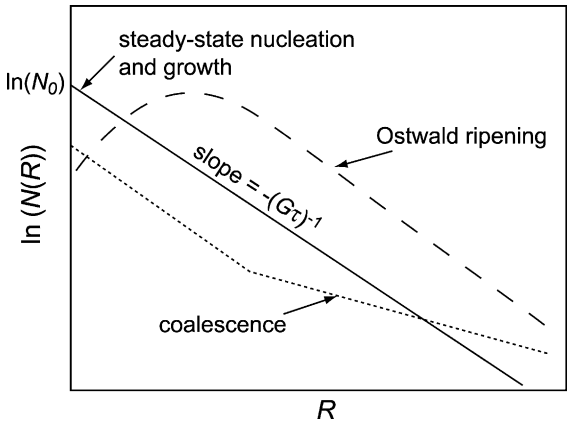

Fig. 1. BSDs predicted by the model of Marsh (1988), after Mangan and Cashman (1996). If steady state nucleation and growth applies (solid line), then a plot of $\ln(N(R))$ versus R is linear with a slope of $-(G\tau)^{-1}$ and intercept of $\ln(N_0)$. Processes which can cause the BSD to deviate from the straight line are: coalescence (dotted line) which increases the proportion of large bubbles and Ostwald ripening which reduces the number of small bubbles (dashed line). Such BSDs were measured in samples of basaltic scoria and reticulite by Mangan and Cashman (1996).

justification for supposing that the BSD is in steady state; this assumption is merely a mathematical convenience. Numerical models of bubble growth due to diffusion and decompression (Sparks, 1978; Proussevitch and Sahagian, 1996; Blower, 2001; Blower et al., 2001b) reveal that growth rates may be far from constant. Although exponential BSDs are commonly observed, measurements also reveal BSDs which deviate strongly from this form (Fig. 1).

2.3. Power law BSDs

A framework for interpreting power law BSDs of volcanic rocks is proposed by Gaonac'h et al. (1996a). In this model the BSD evolves by a mechanism of cascading coalescence. This process is assumed to be scale-invariant and in quasi steady state, giving the relationship:

$$N(V) \propto V^{-B-1} \tag{2}$$

where V is the bubble volume and B is an exponent. (Note that Gaonac'h et al. express the BSD in terms of bubble volume, not radius. The conversion from $N(V)\mathrm{d}V$ to $N(R)\mathrm{d}R$ uses $V \propto R^3$ and $\mathrm{d}V \propto R^2\mathrm{d}R$ and leads to $N(R) \propto R^{-3B-1}$.) The model predicts two regimes: for small bubbles, which are assumed to grow by diffusion and are not affected by coalescence, $B \approx 0$, whereas for medium to large bubbles which are assumed to grow by coalescence, $B \approx 1$ (the 'coalescence regime').

Gaonac'h et al. (1996b) measured BSDs of basaltic lavas from Mount Etna and found that they were in the form represented by Eq. 2. For small vesicles (with areas less than ~ 0.25 mm^2 in thin section) they obtain $B \approx 0$, in agreement with the prediction of the model. For larger vesicles $B \approx 0.85$, close to the predicted value of 1.

2.4. Moments of BSDs

The approach of Toramaru (1989, 1990) and Herd and Pinkerton (1997) does not consider the exact form of the BSD. Instead BSDs are interpreted in terms of readily measurable textural parameters (porosity ϕ, surface area per unit volume S_v, number density N_v and mean bubble radius $\overline{R}$) that are simply related to the moments of the BSD. The ith moment M_i of the BSD is given by:

$$M_i = \int R^i N(R)\mathrm{d}R \tag{3}$$

The first four moments of the BSD are related to the total number of bubbles N, the average bubble radius $\overline{R}$, the total surface area per unit volume S and the total bubble volume per unit volume (i.e. the porosity ϕ):

$$M_0 = N,\ M_1 = \overline{R}N,\ M_2 = \frac{S}{4\pi},\ M_3 = \frac{3\phi}{4\pi} \tag{4}$$

A physical eruption model is still required to quantify how these parameters are related to eruption conditions. Herd and Pinkerton (1997) apply this approach to textural parameters measured in a suite of alkali basalts from recent eruptions on Mount Etna and Stromboli. They conclude that extensive coalescence occurred in samples with $\phi > 35\%$. By contrast, Toramaru (1990) finds that the BSDs observed in pumices from Towada volcano and scoria from Izu–Oshima volcano are not modified by coalescence.

2.5. Experimental samples

Experimental studies of degassing of natural or artificial silicate melts have revealed many important features of the dynamics of bubble nucleation and growth (e.g. Lyakhovsky et al., 1996; Navon et al., 1998; Mourtada-Bonnefoi and Laporte, 1999; Gardner et al., 1999; Liu and Zhang, 2000; Mangan and Sisson, 2000). Generally speaking, however, these experiments do not reproduce the BSDs of natural samples. Usually, a single nucleation event occurs in the experiments and interactions between bubbles are limited, leading to a monodisperse or unimodal BSD (e.g. Lyakhovsky et al., 1996, Gardner et al., 1999).

One exception, however, is the study of Simakin et al. (1999). In their experiments, water-saturated granitic melts were decompressed, causing both vesiculation and crystallisation. BSDs of the experimental samples were compared with those of basaltic scoria from Mount Etna and pumice from Vulcano. Power law BSDs were measured; on combining all the data, the relationship $N(R) \propto R^{-2.8}$ was revealed. It was noted that coalescence took place in only two of the experimental runs, so some mechanism other than that of the cascading coalescence proposed by Gaonac'h et al. (1996a) must have led to the formation of power law BSDs. A plausible explanation lies in the nucleation behaviour in the experiments. Whereas most previous laboratory experiments generated a single episode of nucleation in response to decompression (e.g. Lyakhovsky et al., 1996), Simakin et al. (1999) report that nucleation proceeded in a *continuous* fashion in their experiments. The presence of crystals probably promoted heterogeneous nucleation; previous studies were performed with crystal-free melt and so nucleation would have been more difficult. This mechanism of generating power law BSDs via continuous nucleation will form the crux of the arguments in this paper.

3. The physical model

Experimental studies of the degassing of silicate melts (either natural or synthetic) rarely reproduce the BSDs found in volcanic tephra. However, an analogue system consisting of solutions of gum rosin (natural pine resin) in acetone (GRA) provides a suitable physical model because it closely mimics magmatic degassing behaviour and produces a solid end product which has a very similar texture to that found in many pyroclasts (Fig. 2). The GRA analogue system was first proposed by Phillips et al. (1995). An up-to-date detailed review of the physical properties of the system (viscosity, diffusivity etc.) is presented by Blower (2001).

Gum rosin is an amorphous solid at room temperature and pressure. Solutions of GRA are viscous Newtonian liquids the viscosity of which is strongly dependent on their acetone content, mimicking the analogous dependence of magma viscosity on its water content. During degassing, therefore, the liquid viscosity increases through several orders of magnitude: at 30 wt% acetone the viscosity of the liquid is 0.04 Pa s (Blower, 2001); pure, degassed gum rosin has a viscosity of $\sim 10^{13}$ Pa s (Phillips et al., 1995). This large viscosity increase exerts a strong control on the flow dynamics during degassing (Mourtada-Bonnefoi and Mader, 2001). Volume expansion during vesiculation in both the GRA and magmatic systems depends on the speciation and diffusivity of volatiles and the ratio of initial to final pressure (the decompression ratio). For the experiments presented here, 30 wt% GRA produces the same volume expansion as a silicic magma containing 4 wt% water under eruptions conditions (Lane et al., 2001). The diffusivity of acetone in GRA solutions is of the order 10^{-11} m^2 s^{-1}, similar to measured diffusivities of water in hydrated magmas (Watson, 1994; Zhang and Behrens, 2000) and is dependent on the concentration of acetone (Blower, 2001), just as the diffusivity of water in magma is concentration-dependent (Zhang and Behrens, 2000). A limitation of the small-scale laboratory model is that it cannot replicate the gradual hydrostatic decompression experienced by erupting magma as it rises up a volcanic conduit.

3.1. Experimental procedure

Experiments are performed in a standard shock

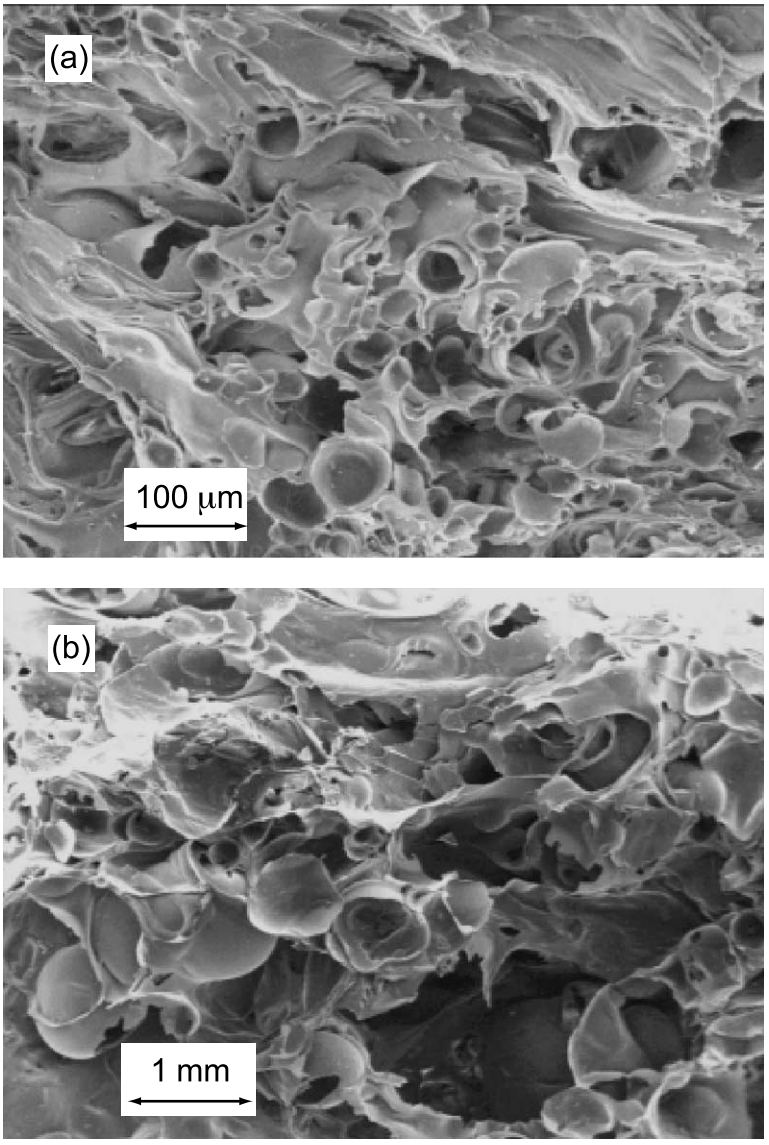

Fig. 2. SEM images of (a) pumice sample from the Minoan Phase 1 Plinian eruption of Santorini, Greece and (b) gum rosin foam. Despite the difference in scales, the images are very similar, depicting highly disordered foams with some spherical and some strained bubbles.

tube apparatus (Fig. 3). The experiments are controlled by two parameters: the initial acetone content of the GRA solution and the pressure in the vacuum chamber. Chamber pressures lower than 200 mbar are required to cause violent degassing on decompression. The initial acetone content controls both the viscosity of the solution and the amount of volatiles available for expansion. The explosivity of the 'eruption' can be increased by increasing the initial acetone content or by decreasing the chamber pressure.

Upon decompression to less than 200 mbar the acetone boils explosively and drives a two-phase flow up the shock tube (Mourtada-Bonnefoi and Mader, 2001). Boiling proceeds as an evaporation wave (Hill and Sturtevant, 1989; Hill, 1991); bub-

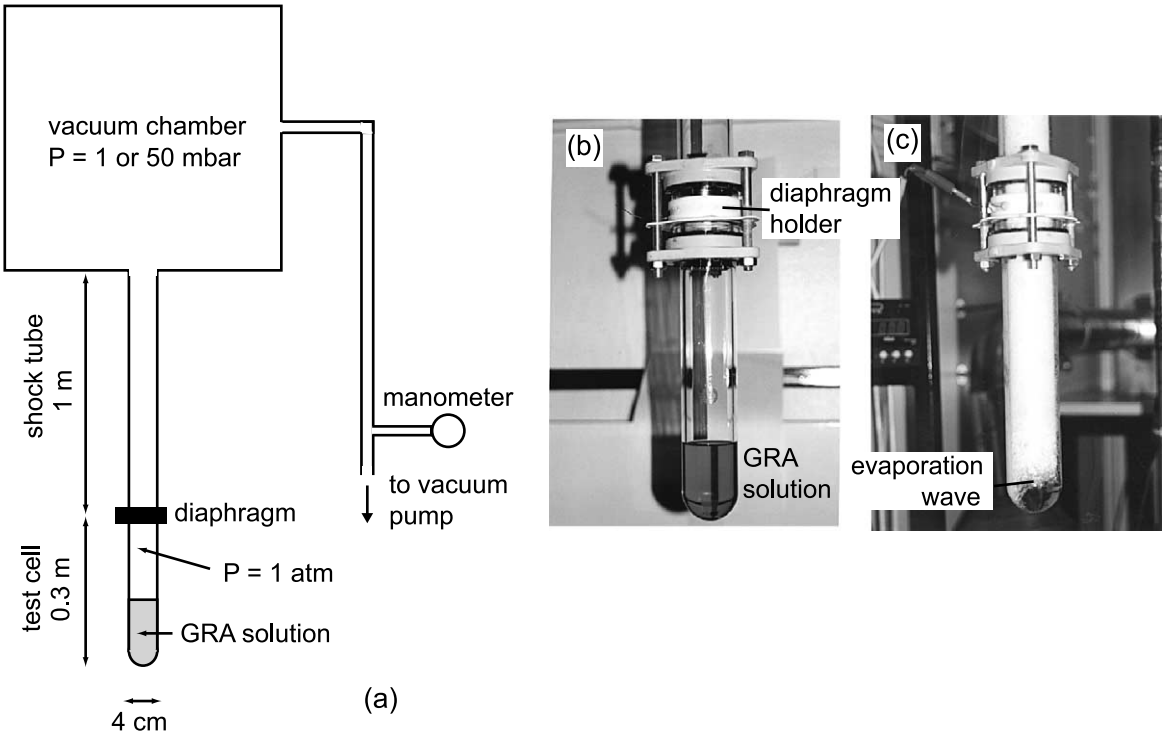

Fig. 3. Experimental apparatus. (a) Schematic diagram of the apparatus used in the GRA decompression experiments. The GRA solution is poured into a cylindrical Pyrex test cell (internal diameter 38 mm and length 300 mm) which is separated by a diaphragm (Sellotape® all-weather tape) from a cylindrical vacuum chamber (height 1 m and diameter 0.5 m). The diaphragm is burst by passing 10 A of current through a length of NiChrome wire around its circumference. This decompresses the solution beneath its boiling pressure (~200 mbar) and initiates the boiling of the acetone. The test cell (b) before and (c) during an experiment. Note that nucleation occurs initially on the surface of the liquid as an evaporation wave.

bles nucleate initially on the surface of the solution and this nucleation surface propagates downward with time (Fig. 3b and c). The bubbly liquid may fragment, depending on the experimental conditions (see Table 1).

After the foam has ceased to expand it is left in the shock tube under vacuum until all the acetone has been removed. The bulk vesicularity of the foam is estimated by measuring the final length L_f of the foam from the base of the test cell to the

Table 1
Summary of experimental conditions in the GRA explosive degassing experiments

Run number	Initial acetone content wt%	Chamber pressure mbar	Foam vesicularity (%)	Fragmentation style
1	30	1.2	89	fragments/spatters
2	30	1.0	89	fragments/spatters
3	25	1.2	91	spatters
4	25	1.0	92	spatters
5	20	50	93	no fragmentation
6	20	50	93	no fragmentation

No fragmentation was observed in experiments 5 and 6. In experiments 3 and 4 the liquid fragmented into 'spatters', i.e. small elongate droplets of bubbly liquid which adhered to the tube walls. Experiments 1 and 2 generated both spatters and fragments; 'fragments' are sub-equant pieces of foam about 1–2 cm across which have separated from the main flow.

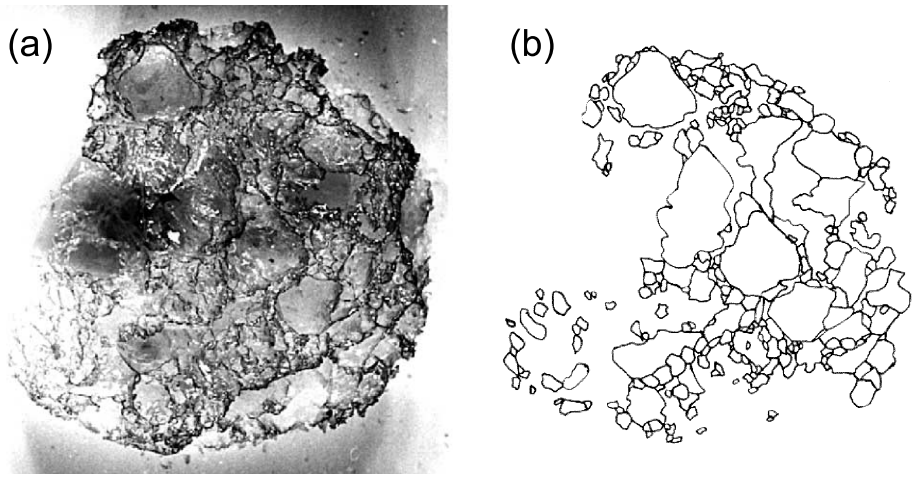

Fig. 4. A slice of gum rosin foam, taken from an experiment in which the initial acetone content was 25 wt% and the chamber pressure was 1 mbar. (a) Image of the slice after partial coating using a gold sputter coater for 30 s. (b) Hand tracing of the image. Width of each image is 3 cm. Note that due to the extreme fragility of the foam many bubble walls have broken during the sectioning process and could not be traced. The hand tracing is scanned into a computer for image analysis.

flow front. The vesicularity of the foam is $(L_f - L_0)/L_0$ where L_0 is the initial depth of solution in the test cell. Cores of dry foam are recovered from the shock tube using a stiff wire to separate the foam from the shock tube wall.

Textural data are extracted from the cores using the following procedure. The gum rosin foam cores are cut into slices around 5 mm thick and 30 mm in diameter using a razor blade and affixed to stiff, white cardboard using PVA glue. The slices are then placed in a gold sputter coater (normally used for coating samples for scanning electron microscopy) for 30 s. This coats the surface of the slice with a thin layer of gold powder. The gold powder appears dark and so contrasts visually with the pale, straw-coloured foam and brings out the shapes of the bubbles. Photographs are taken of the coated slices using monochrome 35-mm film and printed onto A4-sized pieces of high-contrast photographic paper. In this way, images of the slices at a magnification factor of $\sim$6 were generated (Fig. 4). Hand tracings of the bubbles in the photographs are scanned into a computer for computerised image analysis. The software package Visilog® is used to measure the cross-sectional area A of each bubble in the binary images. The equivalent circular radius r of each bubble is then calculated ($r = \sqrt{A/\pi}$).

It was not possible to impregnate the foam to increase its strength and allow the production of a thin section. The foam is highly soluble in all organic solvents (including alcohols) and therefore standard low viscosity resins could not be used. Water-based resins were found to be too viscous, and the surface tension of water too high, to impregnate the foams successfully; furthermore the drying time of these water-based resins was found to be extremely long (several days to weeks).

3.2. Properties of power law BSDs

Power law size distributions are described by the relationship:

$$N(R) \propto R^{-(d+1)} \Rightarrow N(>R) \propto R^{-d} \quad (5)$$

where $N(>R) = \int_R^\infty N(R)dR$ is the number of objects with a radius greater than R, and d is the power law exponent. The cumulative distribution, plotted as $N(>R)$ versus R, is preferable for describing power law BSDs because it produces a more accurate estimate for the exponent, d. This is because the cumulative distribution does not require the data to be separated into arbitrary size classes, which can cause large uncertainties in d.

Power law distributions, unlike unimodal or exponential BSDs (Eqs. 6 and 7), have no characteristic length scale and so no average bubble size in the population. If the exponent d is between 2 and 3 (typical of volcanic rocks as we shall see), then the total volume of the bubbles is controlled mostly by the large bubbles, but the total surface area is controlled by the smallest size fractions (Turcotte, 1992). It is therefore impossible to approximate successfully both diffusive bubble growth (surface area controlled) and decompressive growth (volume controlled) by assuming a monodisperse distribution.

Note that for everything except mathematical fractals, the power law form is only valid for a range of bubble sizes; for the largest and smallest bubbles in a population the power law fit does not in general apply.

3.3. Stereology

Currently, the most widely-used method for measuring the BSD of a volcanic rock is image analysis (Toramaru, 1990; Mangan et al., 1993; Klug and Cashman, 1994; Mangan and Cashman, 1996; Gaonac'h et al., 1996b; Simakin et al., 1999). A thin section (or equivalent) of the rock is made and the resulting slices through the bubbles are analysed. It is common to measure the apparent area A of each bubble on the image and convert this to an equivalent circular radius r ($=\sqrt{A/\pi}$). The task is to deduce the true size distribution $N(R)$ of 3-D bubbles from the measured 2-D distribution $n(r)$ of apparent circle radii; this is the problem of *stereology*. In the Appendix we adopt the converse, forward-modelling approach and provide a method by which the expected distribution of 2-D slices may be calculated from a known 3-D distribution.

If the BSD is monodisperse (i.e. all the bubbles are of the same size), then the problem is trivial. The average radius of the circular slices in thin section is $\bar{r}=(\pi/4)R\approx 0.785R$ where R is the true radius of the bubbles (see Appendix). (Note that the expression $\bar{r}=0.85R\Rightarrow R=1.18\bar{r}$ in Mangan et al. (1993) is incorrect and probably a typographical error; the result in Cashman and Marsh (1988) is correct.)

For the general case of a polydisperse BSD the problem is more complex. Sahagian and Proussevitch (1998) have developed a method for dealing with polydisperse BSDs by considering them to be the sum of many monodisperse distributions. However, although this approach is general and powerful, it is rather unwieldy; unfortunately this is a characteristic problem of all stereological methods.

Here, this problem is circumvented; most of the BSDs we measure are in the form of a power law. This greatly simplifies the stereological method. In the Appendix we show that, if bubbles are spherical and the true BSD is in the form of a power law of the form $N(R)\propto R^{-\alpha}$, then the 2-D distribution of circle slices is of the form $n(r)\propto r^{-(\alpha-1)}$. Therefore, the exponent α of the 3-D distribution is simply one greater than the exponent of the measured 2-D distribution (this fact was also used by Gaonac'h et al., 1996b). It is worth noting that although the analysis in the Appendix is derived using spheres for simplicity, the underlying argument is a purely dimensional one and so this result holds for any bubble shape.

3.4. Experimental results

In order to generate foam from a wide range of experimental conditions, several GRA decompression experiments were performed with a range of initial acetone contents (20, 25 and 30 wt%) and chamber pressures (1 and 50 mbar). Foam from six of these experiments was successfully recovered and analysed. The experimental conditions, foam vesicularities and fragmentation behaviour are summarised in Table 1.

A total of 18 foam slices were made from the foam produced in these experiments, six for each set of experimental conditions. The binary images of the foam slices and the size distributions of the circle slices of the bubbles are shown in Figs. 5–7. In the calculation of the BSD, only circle slices with an area greater than 0.1 mm^2 were used; circle slices smaller than this could not be resolved accurately on the images. Only values of $n(>A)$ greater than 5 were included to ensure that each size class in the analysis was adequately represented.

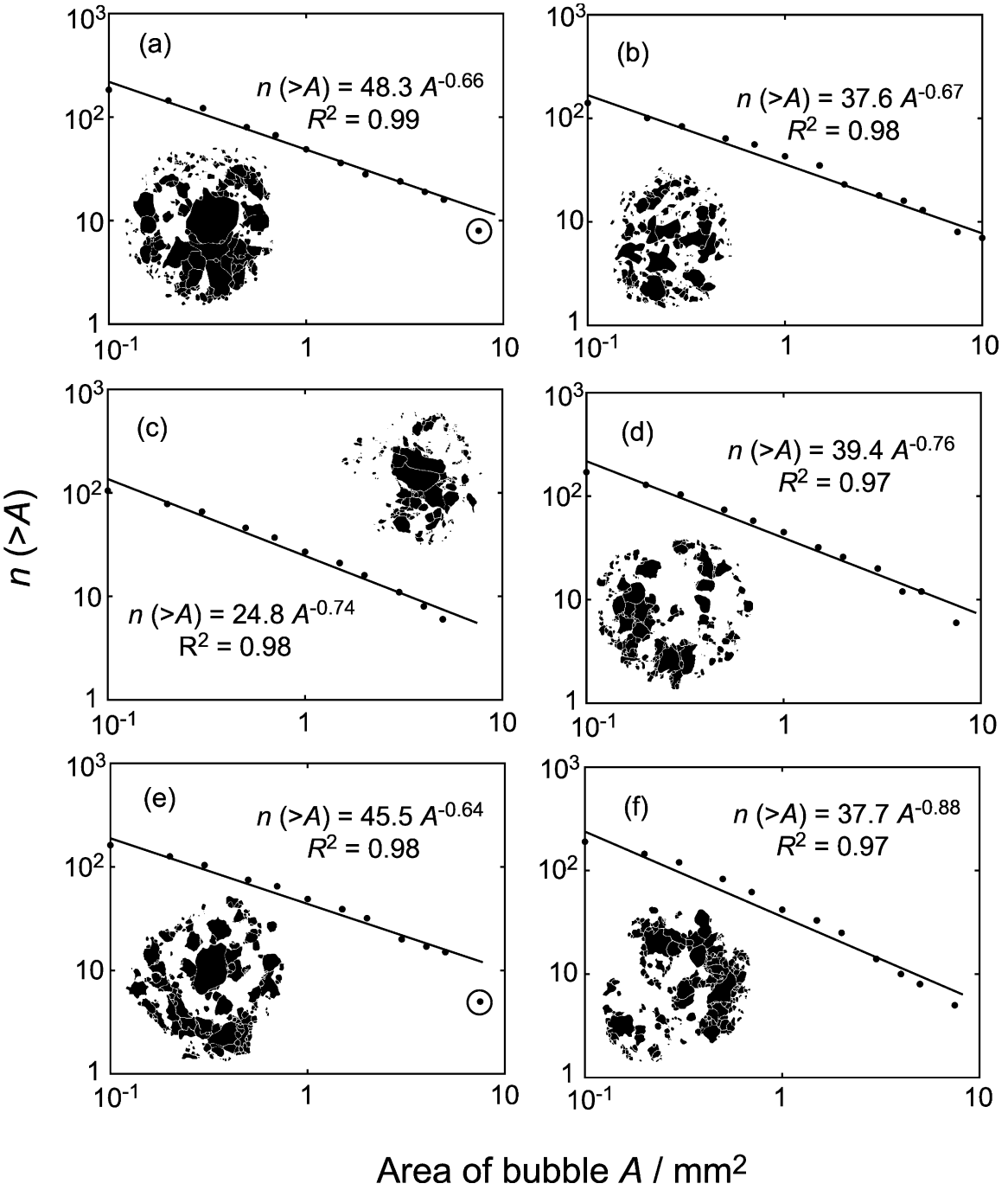

Fig. 5. Cumulative distributions of apparent circle area in sections of six samples from experiments with an initial acetone content of 20 wt% and a chamber pressure of 50 mbar. Samples (a), (b) and (c) are from run 5 (Table 1) and samples (d), (e) and (f) are from run 6. The binary images of the samples are also shown. All six area distributions are well fitted by a power law relationship. Circled points were not included in the calculation of the best fit parameters.

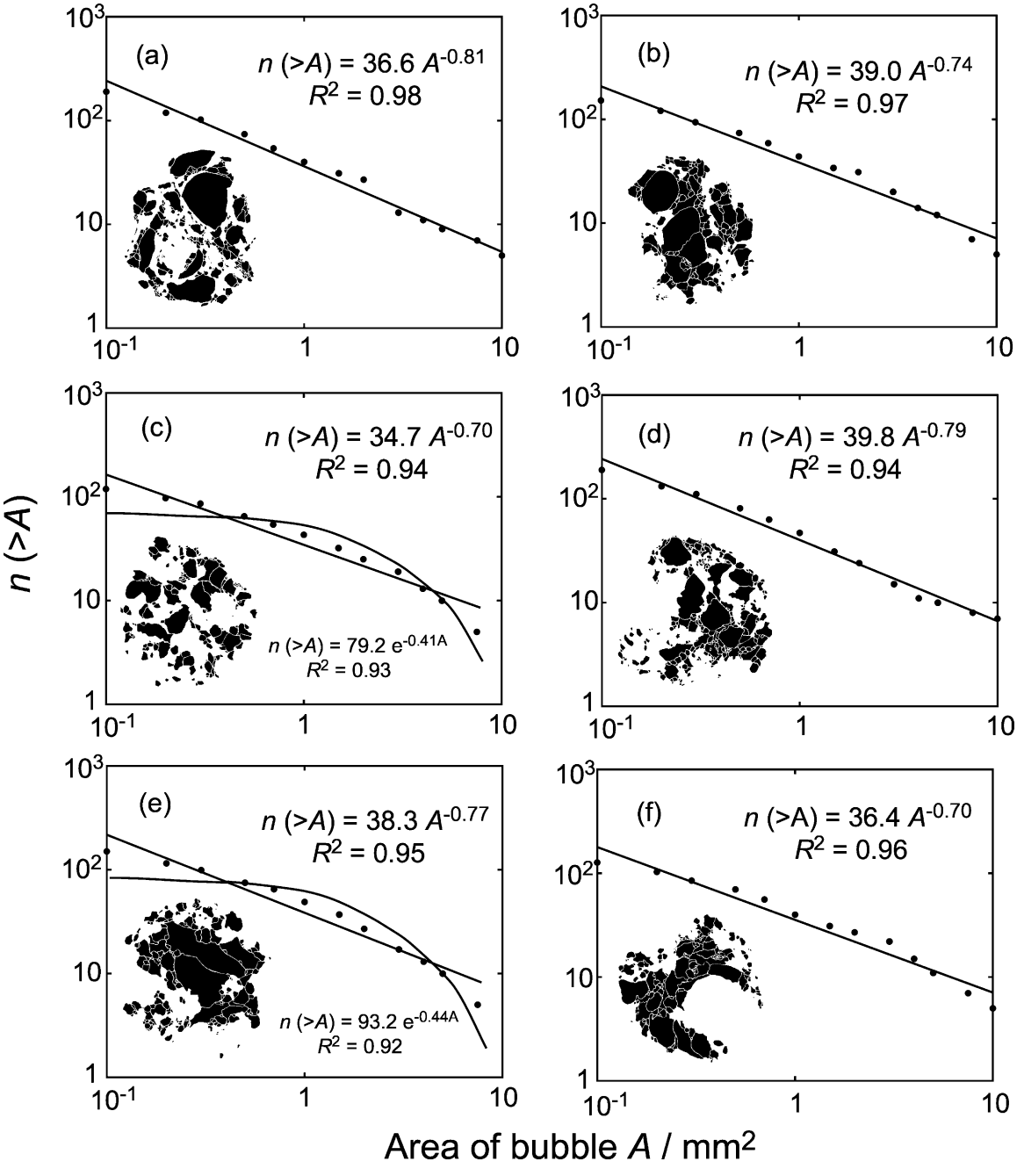

Fig. 6. Cumulative distributions of apparent circle area in sections of six samples from experiments with an initial acetone content of 25 wt% and a chamber pressure of 1 mbar. Samples (a), (b) and (c) are from run 3 (Table 1) and samples (d), (e) and (f) are from run 4. The binary images of the samples are also shown. All six area distributions are well fitted by a power law relationship, but in the case of samples (c) and (e) an exponential distribution is also reasonable.

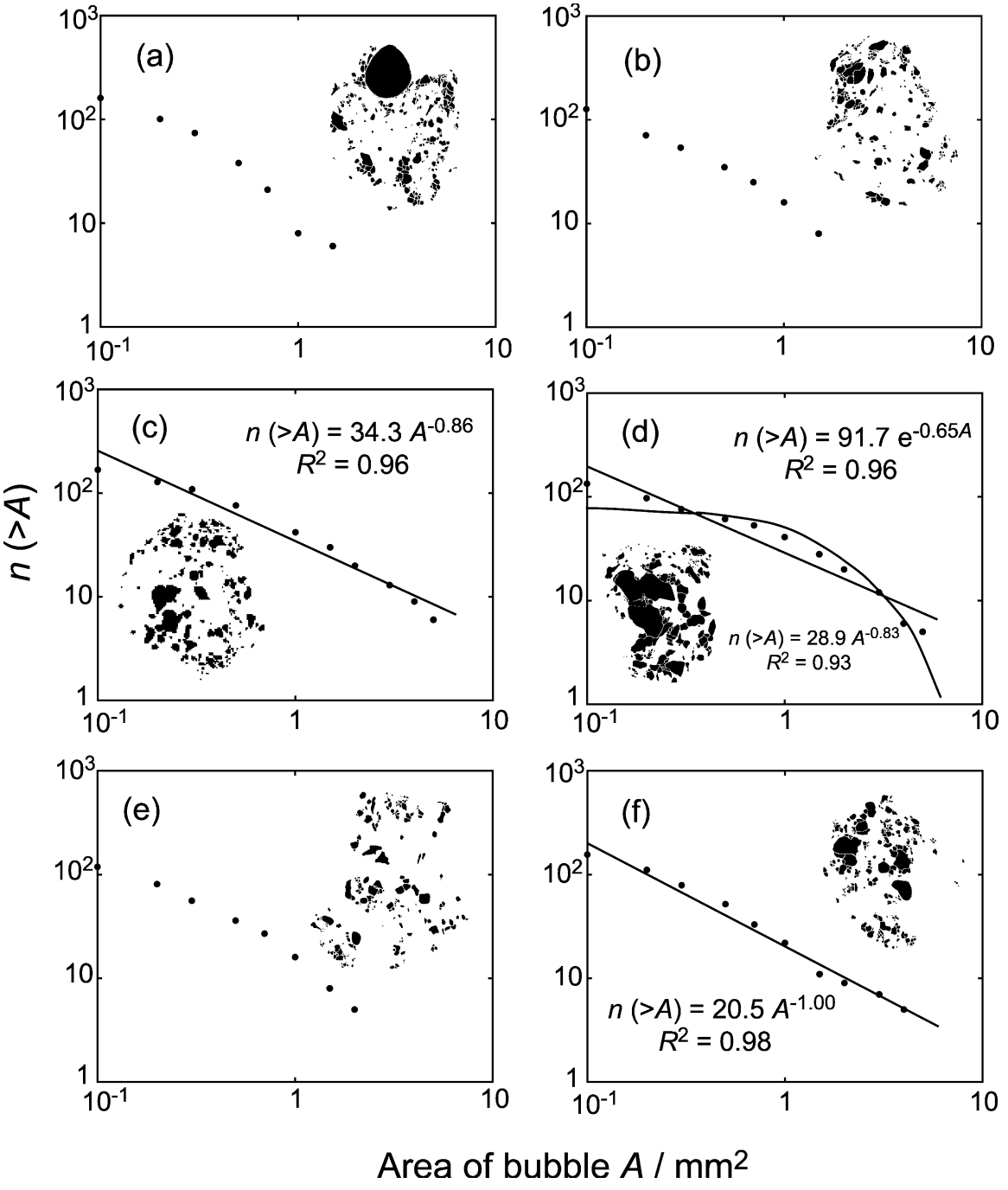

Fig. 7. Cumulative distributions of apparent circle area in sections of six samples from experiments with an initial acetone content of 30 wt% and a chamber pressure of 1 mbar. Samples (a) and (b) are from run 1 (Table 1) and samples (c), (d), (e) and (f) are from run 2. The binary images of the samples are also shown. The area distributions of samples (c) and (e) are well fitted by a power law relationship. The distribution of sample (d) was better fitted by an exponential relationship. The images of samples (a), (b) and (f) were judged to be inadequate for the reliable determination of any particular distribution. The highly explosive nature of the experiments appears to have led to the production of an extremely fragile foam and many bubble walls were broken on sectioning.

Table 2
Summary of results of the BSD analysis of the gum rosin foam

Figure	Sample	R^2 (power law)	R^2 (exponential)	Form of distribution	Power law exponent d
5	(a)	0.99	0.83	power law	2.3
5	(b)	0.98	0.83	power law	2.3
5	(c)	0.98	0.90	power law	2.5
5	(d)	0.97	0.87	power law	2.5
5	(e)	0.98	0.90	power law	2.3
5	(f)	0.97	0.87	power law	2.8
6	(a)	0.98	0.80	power law	2.6
6	(b)	0.97	0.88	power law	2.5
6	(c)	0.94	0.93	(power law)	(2.4)
6	(d)	0.98	0.76	power law	2.6
6	(e)	0.94	0.92	(power law)	(2.5)
6	(f)	0.96	0.89	power law	2.4
7	(c)	0.96	0.92	power law	2.7
7	(d)	0.93	0.96	(exponential)	N/A
7	(f)	0.98	0.83	power law	3.0

For each sample the correlation coefficients (R^2) are shown for both a power law and an exponential fit. For distributions which are well fitted by a power law the exponent d is calculated, with an estimated error of ± 0.2. There is no systematic variation of d with experimental conditions; the differences between the exponents are comparable to the error on the exponent. It can be seen that in most cases a power law distribution gives a much better fit to the data than does an exponential distribution. Brackets denote that the form of the distribution is uncertain, i.e. that the correlation coefficients for power law and exponential fits are similar (within 0.03).

In Figs. 5–7 the power law distributions are expressed in terms of the area of the circle slices, $n(>A) \propto A^{-\lambda}$. Since $A \propto r^2$, the distribution of equivalent circle radii is $n(>r) \propto r^{-2\lambda}$. We have seen that, for a power law distribution, the exponent of the 3-D distribution of bubbles is one greater than that of the 2-D distribution of equivalent circle radii (see 3.3. Stereology). Therefore, $N(>R) \propto R^{-(2\lambda+1)}$, i.e. the power law exponent $d = 2\lambda + 1$. The error in estimating d is difficult to constrain accurately. Some indication of the error can be gained by a bootstrapping method, in which random points from the BSD plot are removed to see how the best fit curve is affected. By this method, the error on the exponent λ was found to be about ± 0.1, giving an error on d of $\sim \pm 0.2$. The results of the analysis are summarised in Table 2.

3.5. Natural samples

We can compare our experimental data with natural samples. A reanalysis of the images in figure 2 of Toramaru (1990) reveals both power law and exponential BSDs in scoria samples from the same basaltic sub-Plinian eruption of Izu–Oshima, Japan (Table 3). The BSDs of pumices from the same figure were found to be generally better described by an exponential distribution.

4. Numerical modelling of power law BSDs

We have seen that BSDs of experimentally generated foam and volcanic rocks of many different types are often in the form of a power law. The work of Gaonac'h et al. (1996a) suggests that a mechanism of cascading coalescence could account for the form of these BSDs. However, in the experiments of Simakin et al. (1999) power law BSDs were generated in the *absence* of bubble coalescence.

In Blower et al. (2001a) we first proposed a model which attributes the formation of power law BSDs to nucleation behaviour, not coalescence. The basis of the model is that nucleation is imagined to proceed in a continuous fashion (as in the experiments of Simakin et al., 1999), simultaneous with growth. Bubbles nucleate and grow

Table 3
BSD analysis of images from figure 2 of Toramaru (1990)

Image	Rock type	R^2 (power law)	R^2 (exponential)	Form of BSD
a	pumice	0.87	0.92	exponential
c	pumice	0.84	0.97	exponential
d	pumice	0.81	0.98	exponential
e	pumice	0.85	0.75	inconclusive
f	pumice	0.91	0.89	inconclusive
g	pumice	0.66	0.90	exponential
h	scoria	0.94	0.68	power law ($d \sim 2.5$)
i	scoria	0.67	0.95	exponential
j	scoria	0.92	0.67	power law ($d \sim 2.5$)
k	scoria	0.94	0.65	power law ($d \sim 2.5$)

Pumice samples came from Towada volcano and scoria samples originated from a basaltic sub-Plinian eruption of Izu–Oshima. The fit of the BSDs to both an exponential and power law form was investigated; the correlation coefficient R^2 is given in each case. If the values of R^2 are similar (within 0.03) or if they are both less than 0.90, then the analysis was deemed to have given an inconclusive result. The scoria samples generally displayed power law BSDs, all with exponents close to 2.5, with one exception (sample i). The pumice samples gave exponential BSDs except for two (e and f) for which the BSD was well fitted by neither an exponential nor a power law. It is important to note that both exponential and power law BSDs have originated from the same eruption. Figure 2b is not included here as it does not contain a sufficient number of bubbles for a reliable reanalysis.

in response to decompression. As magma ascends through the conduit it is continuously decompressed and bubbles continue to nucleate in the pockets of melt between existing bubbles. We will show that this simple mechanism can generate *both* exponential and power law BSDs.

4.1. Fractal models of continuous nucleation

The proposed mechanism in which new generations of bubbles are nucleated and grow in the gaps between pre-existing bubbles can be modelled, in a highly idealised sense, by perfect mathematical constructions which illustrate the emergence of power law distributions.

Perhaps the simplest such construction which leads to a power law BSD is the 1-D *Cantor's middle-third* fractal (Fig. 8a; Falconer, 1984). This starts with a line of unit length, which plays the role of the material. The first step consists of removing the middle third. The gap produced may be thought of as the first-generation bubble. This leaves two segments, each of length one-third. The next step consists of removing the middle third of both of these, producing two new gaps (second-generation bubbles) and leaving four segments, each of length 1/9. Repeating this procedure gives, at the n^{th} step, 2^n segments, each of length $1/3^n$. Taking the limit as $n \to \infty$ produces a fractal. There is clearly one bubble of size 1/3, two of size 1/9, four of size 1/27, and hence 2^{m-1} of size $1/3^m$. Thus, if $L = 1/3^m$, the number of bubbles greater than or equal to L in size is $1+2+4+...+2^{m-1} = 2^m - 1 = L^{-\log 2/\log 3} - 1$, and so $d = \log 2/\log 3 = 0.6309....$

A more realistic construction is the fractal known as the *Apollonian packing* (Falconer, 1984). In 2-D, this fractal is generated by drawing three equal, mutually tangential circles and then filling the curved triangular space in between them with ever-smaller circles (Fig. 8b). The circle size distribution is in the form of a power law with an exponent $d \sim 1.312$ (Fig. 8c). The analogous 3-D figure (a packing of spheres) has $d \sim 2.45$ (Anishchik and Medvedev, 1995). One can readily imagine that these spheres might be bubbles which have nucleated between pre-existing bubbles; in this way the bubbles pack efficiently and fill space. The Apollonian packing has found application particularly in the science of granular materials; it is by definition the densest possible packing of circles (in 2-D) or spheres (in 3-D).

4.2. Developing the model

Although the Apollonian packing represents a useful paradigm, we would not expect natural systems to pack according to such a perfect geome-

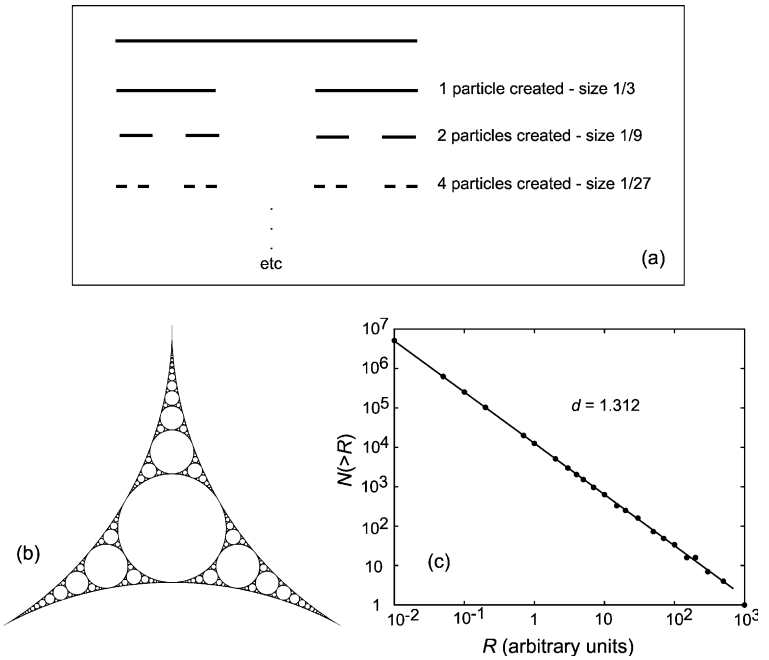

Fig. 8. (a) The Cantor middle-third fractal. (b) The Apollonian packing: starting with three large, touching circles, space is progressively filled with ever-smaller circles. If this procedure is continued ad infinitum then a space-filling fractal is created with no overlap between circles. (c) The distribution of circle sizes in the Apollonian packing.

try. However, we can see evidence of organised space-filling behaviour in textures of natural and experimentally produced foams (Fig. 9). The numerical model which we now develop utilises the process of space-filling nucleation and growth to produce volcanologically realistic textures.

In our model we consider the evolution of the BSD in primarily geometric terms. This approach has the strength that the model is not constrained by timescales and so results can be revealed that are *independent* of the detailed dynamics of the degassing process.

The model works as follows. A small number of bubble nuclei (between 3 and 10 nuclei) are placed at random positions within a 3-D domain. The 'zone of influence' of each bubble is determined, i.e. the volume of the set of points which are closer to the bubble in question than to any other bubble (the *Voronoi cell*). The boundary separating the zones of influence for two neighbouring bubbles is midway between them. In each new time step, a new generation of bubbles nucleates as far as possible from the existing bubbles, at the vertices between Voronoi cells. These are the locations where the volatile resources are least depleted and hence represent the most favourable locations for nucleation (Lyakhovsky et al., 1996). In each time step, the bubbles are allowed to grow according to a parabolic (diffusional) growth law, $R = \beta t^{1/2}$ (Scriven, 1959). The growth constant $\beta = k\sqrt[3]{V_v}$, where k is a constant of proportionality between 0.1 and 0.6 and V_v is the volume of the Voronoi cell. The bubbles grow by an amount $dR = (0.5\beta/\sqrt{t})dt$ where dt equals one time unit and t is given by the number of time steps since nucleation for each bubble. For example, if we are in time step 5 and considering the growth of a bubble that was nucleated in time step 2, then t for that bubble would be 3 dimensionless time units. Thus, bubbles which are relatively isolated and younger grow more rapidly than those which must compete with near neighbours for volatile resources, or are older and so have already depleted the volatiles in their immediate vicinity. Note that there is no explicit length scale; lengths are measured in pixels. The model process is illustrated in Fig. 10.

If two bubbles touch, they cease to grow. This

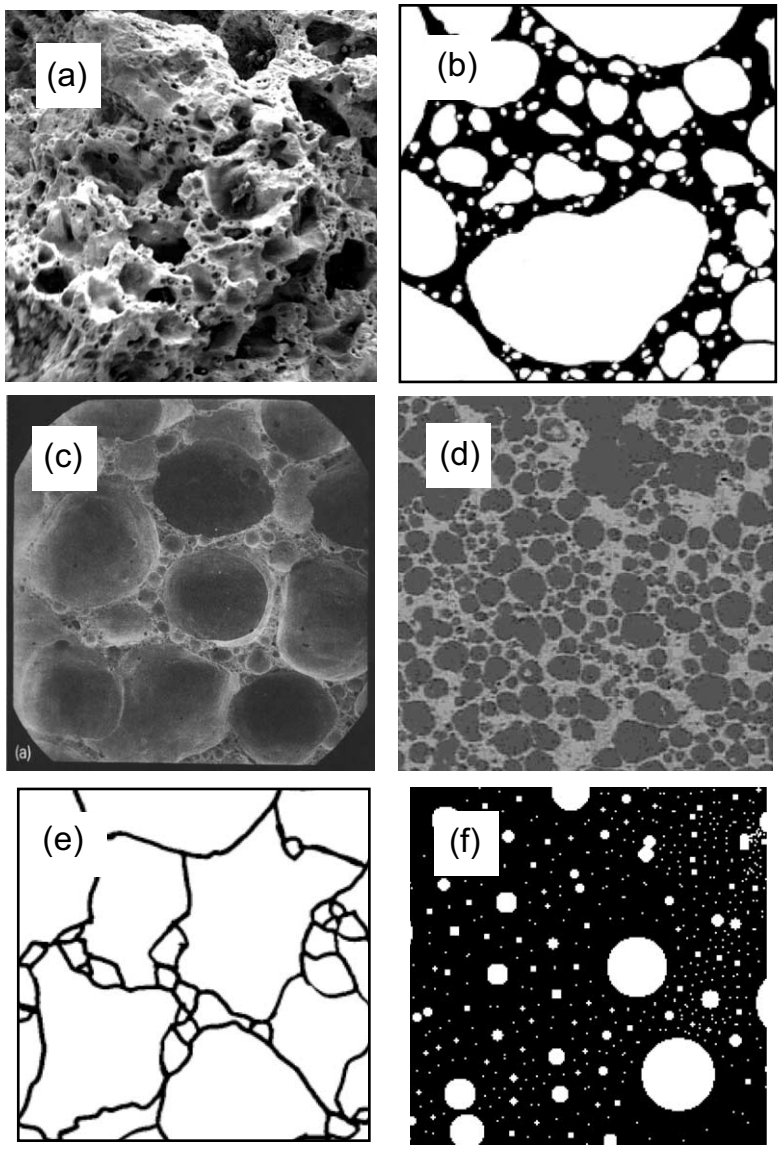

Fig. 9. Illustration of space-filling behaviour in different systems. In each picture several bubble generations are visible with smaller bubbles filling the spaces between larger ones. (a) SEM image of a sample of scoria from the Kokkino cinder cone, Santorini. Image is 7 mm across. (b) Thin section of scoria from a basaltic sub-Plinian eruption of of Izu–Oshima, Japan (reproduced from Toramaru, 1990). Image is 6 mm across. (c) Sample of experimentally produced andesitic foam from figure 8 of Proussevitch et al. (1993). The similarity between this sample and the Apollonian packing (Fig. 8a) is striking. Image is 4 mm across. (d) Sample of experimentally produced foam from figure 3 of Simakin et al. (1999). Image is 4 mm across. (e) Sample of gum rosin foam. The foam vesicularity is very high ($\sim$90%) and so the bubbles are in the form of polyhedral cells. The image is 1.2 mm across. (f) Image of a slice through the 'foam' produced in the numerical model described in the text.

condition was employed to avoid problems of bubble overlap and to prevent bubble coalescence. This constraint is not as unrealistic as it at first appears; since the bubbles are constrained to nucleate as far from each other as possible, they do not begin to touch until late in their evolution, when they would be expected to be approaching their final radius anyway.

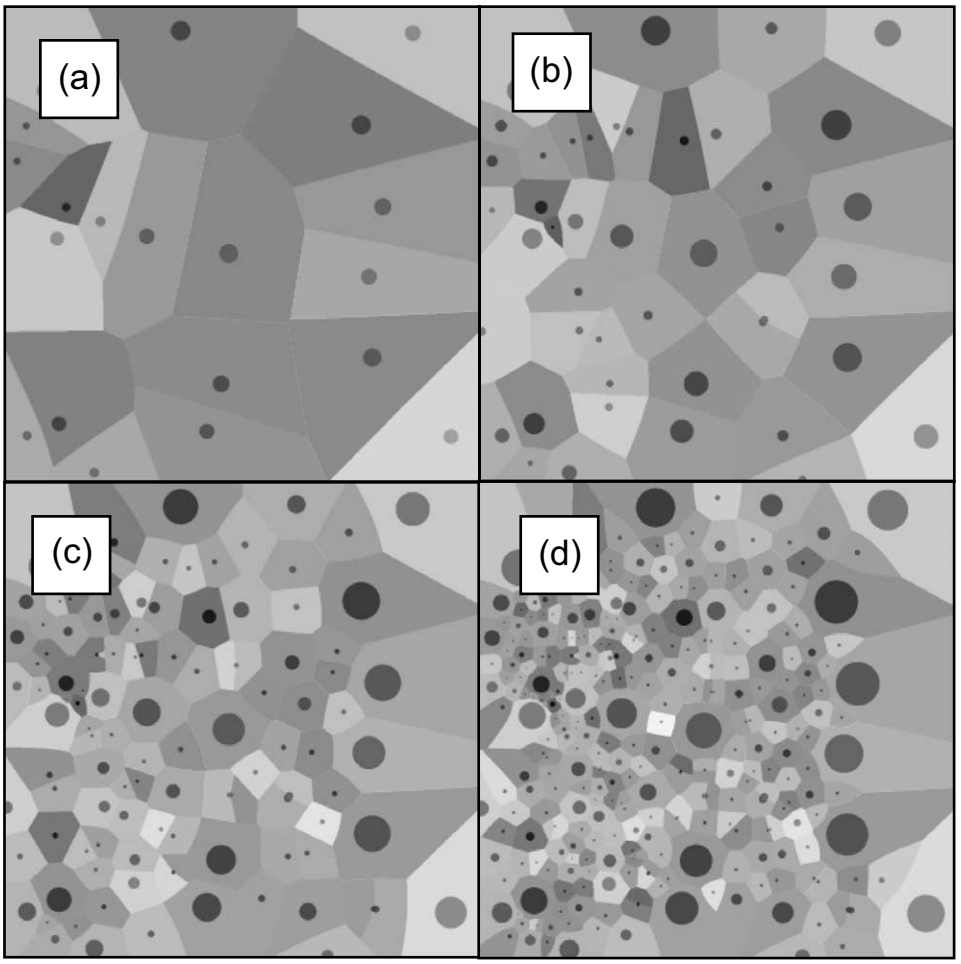

Fig. 10. The construction of the numerical model. For illustrative purposes this diagram shows the results of a two-dimensional version of the model. (a) The initial nucleation event. The bubbles have been allowed to grow by a small amount. The shades of grey represent the Voronoi cells of different bubbles. (b) The second generation bubbles have nucleated at the vertices between the Voronoi cells in the first picture. The Voronoi cells have been recalculated. (c) and (d) Two more stages in the evolution of the bubble distribution.

4.3. Results of the numerical model

The main result of the model is that the form of the BSD depends most strongly on the number of nucleation events which occur during growth. If there is only one nucleation event a unimodal BSD results (Fig. 11). Because of the dependence of the growth rate β on the Voronoi volume, the size of each bubble depends on the proximity of its neighbours. Under the simplifying assumption that the final bubble size is proportional to the distance to the nearest bubble, a Poisson distribution is expected (Tuckwell, 1988):

$$N(R) \propto R^2 \exp(-\lambda R^3) \Rightarrow N(>R) \propto \exp(-\lambda R^3) \qquad (6)$$

where λ is a constant related to the number density of bubble nuclei.

After a small number (typically 3) nucleation events have occurred, an exponential BSD emerges (Fig. 11a):

$$N(R) \propto \exp(-R/R_0) \Rightarrow N(>R) \propto \exp(-R/R_0) \qquad (7)$$

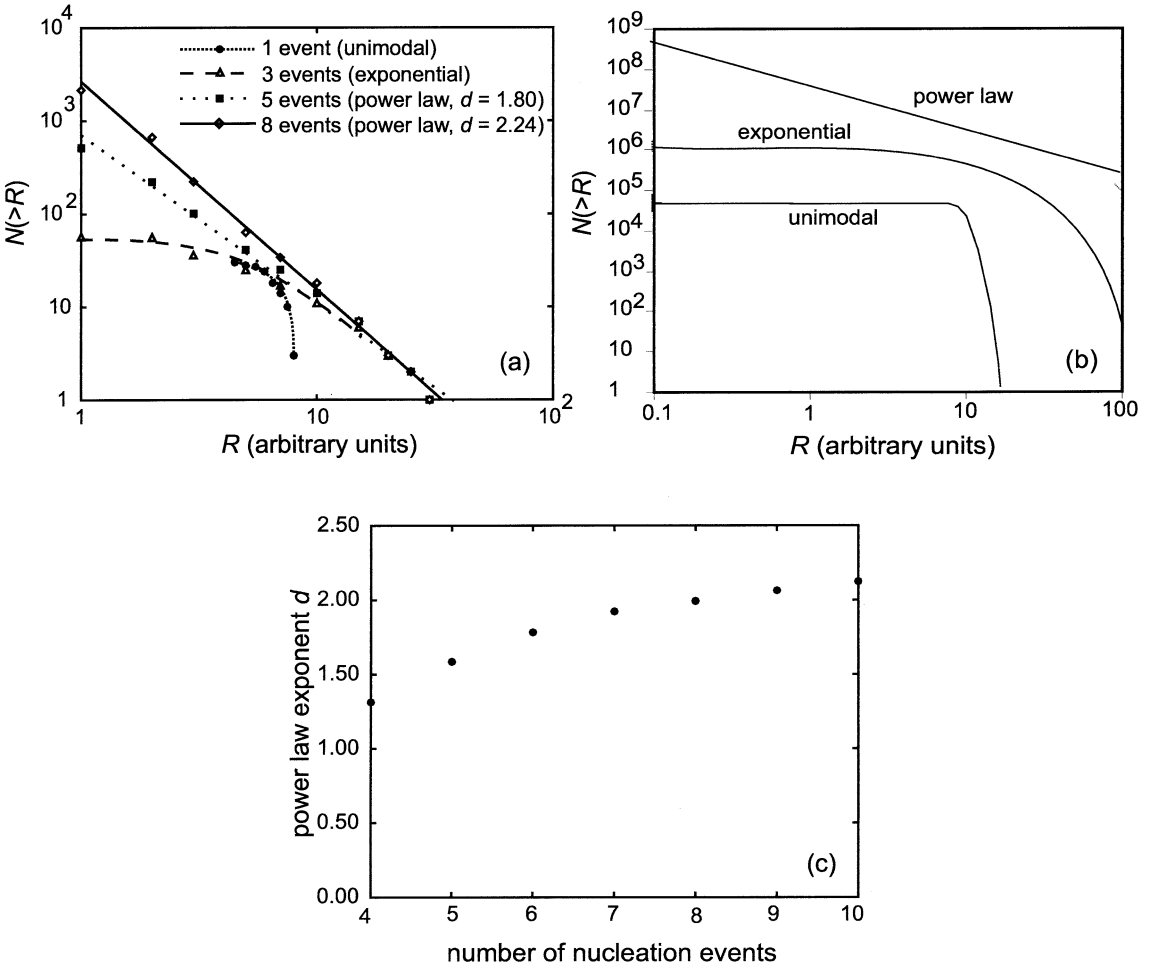

Fig. 11. Results of a typical model run. (a) Plots of $N(>R)$ versus R at different stages during a model run. A single nucleation event gives a unimodal BSD. After three events the BSD has taken an exponential form (with correlation coefficient 0.97). Five events give a power law BSD with exponent $d=1.80$ (with correlation coefficient 0.99). After eight events the BSD is still in the form of a power law, but the exponent has increased to 2.24 (with correlation coefficient 0.99). The BSD is evolving throughout the model run and is therefore not in steady state (cf. Marsh, 1988). (b) In (a), the number of bubbles with a radius greater than R is plotted against R (i.e. the cumulative distribution) on double-logarithmic axes and so some of the BSDs appear unfamiliar. This plot shows for comparison the curves for perfect unimodal, exponential and power law cumulative distributions. (c) The evolution of the power law exponent d with successive nucleation events in a typical model run. After four nucleation events the BSD is intermediate between an exponential and power law form. For five events and greater the BSD is power law in form; the exponent increases with the number of nucleation events.

(see Eq. 1) where R_0 is a characteristic bubble size. Note that the model predicts exponential BSDs without the assumption of a steady state BSD or a constant bubble growth rate (see Marsh, 1988). In the model, exponential BSDs always evolve into power law distributions (Eq. 5) with further nucleation events. After a total of about 5 events the distribution is consistently power law (Fig. 11a). As more nucleation events occur, the distribution remains in the form of a power law, but the exponent d increases with the number of events (Fig. 11b).

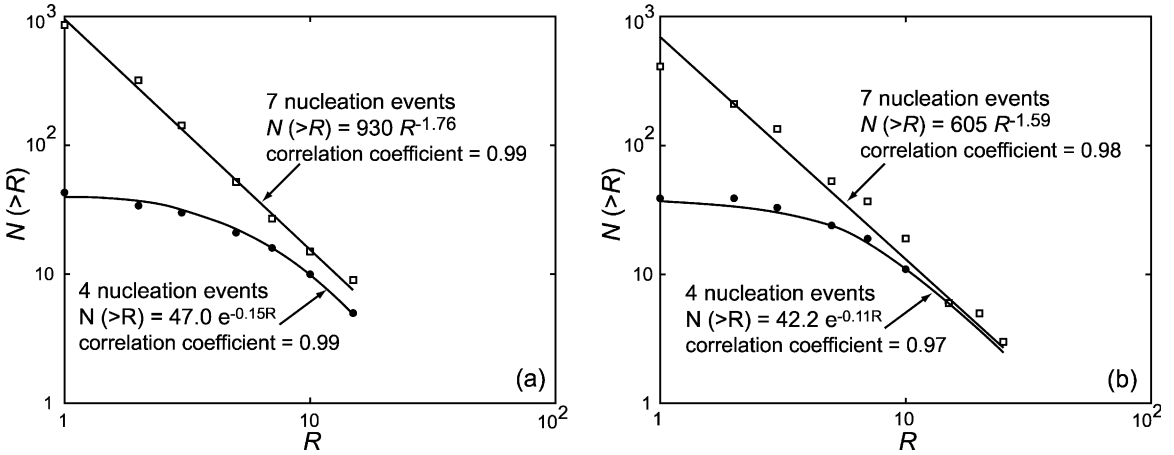

Fig. 12. The effect of the growth law and nucleation rate. (a) The results of a model run in which bubbles grew according to a linear growth law, $r \propto t$. An exponential BSD is produced after four nucleation events; a power law distribution is observed after seven events. The initial unimodal distribution has been omitted from this diagram for clarity. (b) The results of a model run in which only half of the Voronoi vertices were populated with new nuclei in each time step, simulating a slower nucleation rate. Once more, an exponential BSD is produced after four nucleation events; a power law distribution is observed after seven events.

4.4. The effect of the bubble growth law and nucleation rate

So far we have used a parabolic (diffusional) growth law for bubbles. This growth law has been shown to be an oversimplification, particularly for high-viscosity melts (Proussevitch and Sahagian, 1996; Lyakhovsky et al., 1996; Blower, 2001, Blower et al., 2001b). Other growth laws may be used in the model, and the main results are unaffected. Fig. 12a shows the results of a model run in which the bubbles grew according to a linear growth law, $R \propto t$, as deduced from the bubble growth model of Blower et al. (2001b). A single nucleation event gives a unimodal distribution as before. After 4 nucleation events the BSD is exponential in form. A power law distribution is generated after 7 events. Between these times the distribution is intermediate between an exponential and a power law form and the BSD may be equally well fitted by either form. This insensitivity of the results to the bubble growth law is due to the fact that the BSD is constrained mainly by the *geometry* of the system; the details of the vesiculation process do not affect this fundamental property.

This observation provides the justification for using a numerical procedure in which the volume of melt is not conserved. Conservation could be achieved by rescaling the domain after each time step so that the melt volume remained constant. This would have the effect of changing the growth law for the bubbles. But, as we have seen above, the growth law has no significant effect on the form of the BSD.

In the model described so far, each nucleation event populates all Voronoi vertices with new bubble nuclei. The 'nucleation rate' may be altered by only populating a certain fraction of the vertices in each event. Again, this has very little effect on the main results of the study. Fig. 12 shows the results of a model run in which only half of the Voronoi vertices were populated with new nuclei in each time step. A progression through an exponential BSD (4 nucleation events) to a power law BSD (7 events) is once more produced.

5. Discussion and conclusions

The numerical model demonstrates that unimodal, exponential and power law BSDs can be generated by a mechanism of continuous nucle-

ation and in the absence of bubble coalescence. The analogue experiments (see 3. The physical model) have also generated power law BSDs. One characteristic of the experiments is that the degassing is highly non-equilibrium. The pressure drop is extremely rapid and the volatile (acetone) content of the solution is high; it is therefore impossible for all the acetone to be lost from the solution on the timescale of decompression. This is borne out by observation; the residual acetone content of the foam immediately after expansion ceases is significant (Mourtada-Bonnefoi and Mader, 2001). The foam becomes sufficiently permeable to allow these residual volatiles to escape without any further expansion.

5.1. Non-equilibrium degassing and continuous nucleation

The combined results of the analogue experiments and numerical modelling suggest that the presence of a power law or exponential BSD is indicative of a degassing system that cannot maintain equilibrium with its environment. The observed evaporation wave that propagates through the liquid marks the start of the nucleation process. If the diffusive mass transfer of volatile molecules into the first bubble population nucleated on the surface of the solution as this wave passes is not rapid enough to allow the system to maintain a volatile concentration in the melt which is in equilibrium with the ambient pressure then further bubbles may nucleate in the volatile-rich melt pockets between bubbles (Lyakhovsky et al., 1996). Such nucleation behaviour has been reported in experiments simulating the degassing of silicate melts (Navon et al., 1998; Simakin et al., 1999). As a result of this non-equilibrium degassing, continuous bubble nucleation occurs and a power law BSD is generated. Power law or exponential BSDs are to be expected whenever a system is forced far from equilibrium and physical parameters do not favour efficient degassing, i.e. for rapid depressurisation, low initial nucleation density, and slow volatile diffusion. The exponent d is a measure of the number of nucleation events, or the length of the nucleation period relative to the timescale of growth. Non-equilibrium degassing has been shown to be significant during the early stages of degassing in volcanic melts (Gardner et al., 1999; Simakin and Salova, 2001).

5.2. Theoretical remarks

The fact that the first generation BSD is Poissonian is a direct consequence of the two assumptions: that the nucleation sites of the first bubble population are randomly distributed, and that the bubbles grow at a rate which increases with the distance to the nearest neighbour. This would thus seem to be a robust conclusion. The fact that the BSD is a power law after several nucleation generations is a consequence of the scale-invariance, and hence loss of a characteristic length, which results from repeated nucleation of bubbles on smaller and smaller scales in the gaps between earlier generations of bubbles, as in both the Apollonian packing and Cantor's middle-third constructions discussed in 4.1. Fractal models of continuous nucleation. This, too, would thus appear to be a robust conclusion. Consideration of the curves in Fig. 11 might lead one to expect that the transition between these extremes would be approximately exponential in form. That it is consistently so close to being exactly exponential is, however, surprising. We know of no explanation for this observation.

5.3. Coalescence versus continuous nucleation

The mechanism of producing power law BSDs by means of continuous nucleation does not incorporate the effects of coalescence. In an effusive eruption involving low viscosity magma, we might expect that degassing will be close to equilibrium, and so the likelihood of the occurrence of several nucleation events is much reduced. The mechanism of cascading coalescence (Gaonac'h et al., 1996a) may therefore be dominant in generating power law BSDs in basaltic lavas (Gaonac'h et al., 1996b).

By contrast, in the case of explosive eruptions, especially involving acidic, highly viscous magma and rapid magma ascent rates, bubble growth models (Proussevitch and Sahagian, 1996; Blower, 2001; Blower et al., 2001b) predict non-equi-

librium degassing and so continuous nucleation may occur. There is strong evidence that both exponential and power law BSDs can be generated in the absence of coalescence (e.g. Simakin et al., 1999; Toramaru, 1990). We interpret these pre-coalescence BSDs to be the result of multiple nucleation events.

A point which has yet to be resolved is the problem of why laboratory experiments in which silicate melts are degassed do not in general produce continuous nucleation (e.g. Lyakhovsky et al., 1996; Gardner et al., 1999). This is probably due to a difficulty in nucleation; most laboratory systems investigate crystal-free melt. However, Simakin et al. (1999) allowed crystallisation to occur in their experiments and did indeed observe continuous nucleation. The experiments of Proussevitch et al. (1993) are particularly instructive. They investigated the degassing of andesitic and rhyolitic melt. The rhyolitic samples were crystal-free and did not produce a characteristic space-filling pattern of bubbles. However, the andesitic samples contained about 7% quartz particles; the texture of the foam produced (Fig. 9c) strongly implies that continuous nucleation occurred in this case.

5.4. Implications for modelling volcanic processes

Our findings may resolve an apparent contradiction in current numerical models of explosive volcanic eruptions. Conduit flow models (Papale et al., 1998; Melnik and Sparks, 1999) are usually based on the assumption that degassing is an equilibrium process. By contrast, bubble growth models (Proussevitch and Sahagian, 1996) assume a single nucleation event and a monodisperse BSD and predict non-equilibrium degassing under the conditions of an explosive eruption, in agreement with our observations. However, highly non-equilibrium conditions are expected to lead to continuous nucleation. This would tend to increase the efficiency of the degassing process and allow the system to remain close to equilibrium. The process of continuous nucleation can explain why the assumptions behind conduit flow models can also be consistent with non-equilibrium degassing.

Acknowledgements

We thank Fred Wheeler and Mike Dury for technical assistance with the building of the shock tube. We are grateful to Catherine Mourtada-Bonnefoi and Steve Sparks for helpful discussions and to Alex Proussevitch and Alexander Simakin for insightful reviews. Jon Keating and Heidy Mader enjoyed the generous hospitality of the American Institute of Mathematics, Palo Alto, CA, USA, during the writing of this article. Jon Blower was supported by a NERC studentship, reference GT 04/97/26/E3. The research was partially funded by the EC–Network project ENV4-0703.

Appendix. Stereology

Given a distribution $N(R)$ of randomly placed spheres in 3-D space, we wish to find the expected distribution $n(r)$ of circular slices resulting from the intersection of a plane and the spheres. It is natural to approach this problem in terms of probability theory and so we here use the probability density functions $F(R)$ and $f(R)$ for the 3-D and 2-D distributions, respectively. The probability density function is simply a dimensionless number density function obtained by normalising the number density function with respect to the total number of bubbles, i.e. $N(R) = N_T F(R)$ and $n(R) = n_T f(R)$ where N_T is the total number of bubbles and n_T is the total number of circles.

Fig. A1 shows the intersection of a spherical bubble of radius R and a plane distant x from the bubble centre. The radius of the circle described by the intersection of the plane and the sphere is r, where:

$$r = \sqrt{R^2 - x^2} \tag{A.1}$$

A.1. Monodisperse BSD

The simplest case, which shall be dealt with first, is that of a monodisperse distribution (i.e. all the bubbles have the same radius). If these bubbles are randomly positioned, then a slice through the population will generate a range of circle sizes; some bubbles will be intersected near

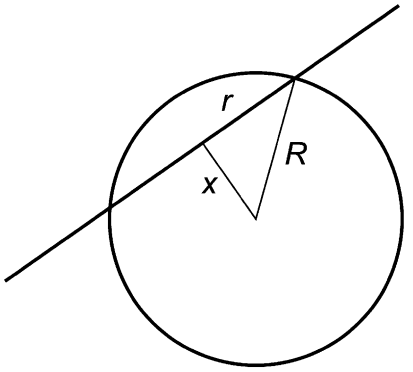

Fig. A.1. The intersection of a spherical bubble of radius R with a plane at a distance x from the bubble centre. The radius of the circular slice of the bubble in the plane is r.

a diameter and will appear as a circle of radius $\sim R$, whilst others will be intersected away from a diameter and will appear as smaller circles.

From equation A.1:

$$x = \sqrt{R^2 - r^2} \Rightarrow \frac{\mathrm{d}x}{\mathrm{d}r} = -\frac{r}{\sqrt{R^2 - r^2}} \tag{A.2}$$

From the laws of probability:

$$|f(x)\mathrm{d}x| = |f(r)\mathrm{d}r| \Rightarrow f(r) = f(x)\left|\frac{\mathrm{d}x}{\mathrm{d}r}\right| \tag{A.3}$$

where $f(r)$ and $f(x)$ are the probability density functions of r and x, respectively.

Now, since each value of x has an equal chance of occurring and $0 \le x \le R$, $f(x) = 1/R$. Therefore:

$$f(r) = \frac{1}{R}\frac{r}{\sqrt{R^2 - r^2}} \tag{A.4}$$

Fig. A2 shows the form of the expected 2-D slice distribution in the case of a monodisperse BSD. The average slice radius $\bar{r}$ is given by:

$$\bar{r} = \int_0^R r f(r)\mathrm{d}r = \frac{1}{R}\int_0^R \frac{r^2}{\sqrt{R^2 - r^2}}\,\mathrm{d}r = \frac{\pi}{4}R \tag{A.5}$$

A.2. Polydisperse BSDs – the general case

Eq. A.4 gives the probability of obtaining a circular cross-section of radius r given the intersection of a plane with a sphere of radius R. Now let us consider a polydisperse distribution of bubbles with probability density function $F(R)$. The probability of a plane intersecting a given bubble is proportional to the bubble radius R. Cross-sections of radius r may be obtained from any bubble with a radius greater than or equal to r. We may now write a general expression for the probability of obtaining a cross-section of radius r from the whole distribution:

$$f(r) = \int_r^\infty F(R) R \frac{1}{R}\frac{r}{\sqrt{R^2 - r^2}}\,\mathrm{d}R \tag{A.6}$$

That is to say, $f(r)$ is the probability of finding a bubble of radius R, multiplied by the probability of intersecting this bubble, multiplied by the probability of obtaining a slice of radius r from this bubble, integrated over the range of $R \ge r$. This gives:

$$f(r) = \int_r^\infty \frac{r}{\sqrt{R^2 - r^2}} F(R)\,\mathrm{d}R \tag{A.7}$$

A.2.1. Power law (fractal) BSD

The general form of a power law (or fractal) BSD is:

$$F(R) = aR^{-\alpha} \tag{A.8}$$

where a is a constant and α is the power law exponent. From Eq. A.7:

$$f(r) = \int_r^\infty \frac{r}{\sqrt{R^2 - r^2}} aR^{-\alpha}\mathrm{d}R \tag{A.9}$$

Substituting $R = ry$ (which implies $\mathrm{d}R = r\mathrm{d}y$):

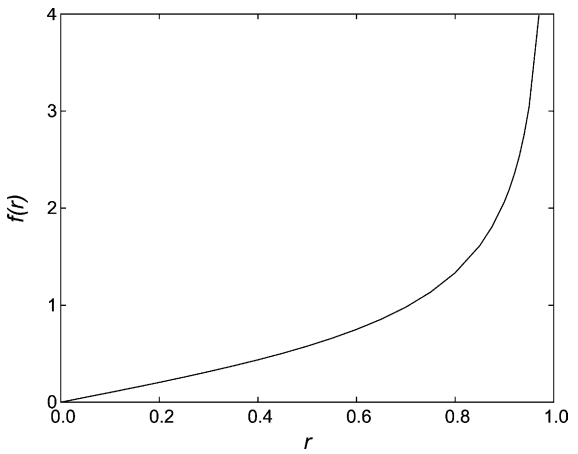

Fig. A.2. The expected 2-D probability density function, $f(r)$, of circles produced by the intersection of a plane with a randomly placed, monodisperse distribution of spheres of unit radius.

$$f(r) = a\int_1^\infty \frac{r}{\sqrt{r^2y^2-r^2}}(ry)^{-\alpha} r\mathrm{d}y =$$

$$ar^{1-\alpha}\int_1^\infty \frac{y^{-\alpha}}{\sqrt{y^2-1}}\,\mathrm{d}y \qquad (A.10)$$

Noting that the integral factor is independent of r, we obtain:

$$f(r) \propto r^{-(\alpha-1)} \qquad (A.11)$$

This is an important result; it implies that if the size distribution of bubbles is in the form of a power law with exponent α, then the size distribution of slices is also in the form of a power law with an exponent of $(\alpha-1)$.

References

Anishchik, S.V., Medvedev, N.N., 1995. Three-dimensional Apollonian packing as a model for dense granular systems. Phys. Rev. Lett. 75, 4314–4317.

Blower, J.D., 2001. Degassing Processes in Volcanic Eruptions. Ph.D. Thesis, University of Bristol.

Blower, J.D., Keating, J.P., Mader, H.M., Phillips, J.C., 2001a. Inferring volcanic degassing processes from vesicle size distributions. Geophys. Res. Lett. 28, 347–350.

Blower, J.D., Mader, H.M., Wilson, S.D.R., 2001b. Coupling of viscous and diffusive controls on bubble growth during explosive volcanic eruptions. Earth Planet. Sci. Lett., in press.

Burnard, P., 1999. Eruption dynamics of 'popping rock' from vesicle morphologies. J. Volcanol. Geotherm. Res. 92, 247–258.

Cashman, K.V., Marsh, B.D., 1988. Crystal size distribution (CSD) in rocks and the kinetics and dynamics of crystallization, II. Makaopuhi lava lake. Contr. Mineral. Petrol. 99, 292–305.

Falconer, K.J., 1984. The Geometry of Fractal Sets. Cambridge Tracts in Mathematics 85, Cambridge University Press, Cambridge.

Gaonac'h, H., Lovejoy, S., Stix, J., Schertzer, D., 1996a. A scaling growth model for bubbles in basaltic lava flows. Earth Planet. Sci. Lett. 139, 395–409.

Gaonac'h, H., Stix, J., Lovejoy, S., 1996b. Scaling effects on vesicle shape, size and heterogeneity of lavas from Mount Etna. J. Volcanol. Geotherm. Res. 74, 131–153.

Gardner, J.E., Hilton, M., Carroll, M.R., 1999. Experimental constraints on degassing of magma: Isothermal bubble growth during continuous decompression from high pressure. Earth Planet. Sci. Lett. 168, 201–218.

Herd, R.A., Pinkerton, H., 1997. Bubble coalescence in basaltic lava: Its impact on the evolution of bubble populations. J. Volcanol. Geotherm. Res. 75, 137–157.

Hill, L.G., Sturtevant, B., 1989. An experimental study of evaporation waves in a superheated liquid. In: Meier, G.E.A., Thompson, P.A. (Eds.), Adiabatic waves in liquid–vapour systems. IUTAM Symposium Göttingen, Springer, pp. 25–37.

Hill, L.G., 1991. An Experimental Study of Evaporation Waves in a Superheated Liquid. Ph.D. Thesis, California Institute of Technology, CA.

Klug, C., Cashman, K.V., 1994. Vesiculation of May 18, 1980, Mount St. Helens magma. Geology 22, 468–472.

Lane, S.J., Chouet, B.A., Phillips, J.C., Dawson, P., Ryan, G.A., Hurst, E., 2001. Experimental observations of pressure oscillations and flow regimes in an analogue volcanic system. J. Geophys. Res. 106, 6461–6476.

Liu, Y., Zhang, Y., 2000. Bubble growth in rhyolitic melt. Earth Planet. Sci. Lett. 181, 251–264.

Lyakhovsky, V., Hurwitz, S., Navon, O., 1996. Bubble growth in rhyolitic melts: Experimental and numerical investigation. Bull. Volcanol. 58, 19–32.

Mangan, M.T., Cashman, K.V., 1996. The structure of basaltic scoria and reticulite and inferences for vesiculation, foam formation, and fragmentation in lava fountains. J. Volcanol. Geotherm. Res. 73, 1–18.

Mangan, M.T., Cashman, K.V., Newman, S., 1993. Vesiculation of basaltic magma during eruption. Geology 21, 157–160.

Mangan, M., Sisson, T., 2000. Delayed, disequilibrium degassing in rhyolite magma: Decompression experiments and implications for explosive volcanism. Earth Planet. Sci. Lett. 183, 441–455.

Marsh, B.D., 1988. Crystal size distribution (CSD) in rocks and the kinetics and dynamics of crystallization, I. Theor. Contr. Mineral. Petrol. 99, 277–291.

Melnik, O.E., Sparks, R.S.J., 1999. Nonlinear dynamics of lava dome extrusion. Nature 402, 37–41.

Mourtada-Bonnefoi, C.C., Laporte, D., 1999. Experimental study of homogeneous bubble nucleation in rhyolitic magmas. Geophys. Res. Lett. 26, 3505–3508.

Mourtada-Bonnefoi, C.C., Mader, H.M., 2001. On the development of highly-viscous skins of liquid around bubbles during magmatic degassing. Geophys. Res. Lett. 28, 347–350.

Navon, O., Chekhmir, A., Lyakhovsky, V., 1998. Bubble growth in highly viscous melts: theory, experiments, and autoexplosivity of dome lavas. Earth Planet. Sci. Lett. 160, 763–776.

Orsi, G., Gallo, G., Heiken, H., Wohletz, K., Yu, E., Bonani, G., 1992. A comprehensive study of pumice formation and dispersal: The Cretaio Tephra of Ischia Italy. J. Volcanol. Geotherm. Res. 53, 329–354.

Papale, P., Neri, A., Macedonio, G., 1998. The role of magma composition and water content in explosive eruptions, 1. Conduit ascent dynamics. J. Volcanol. Geotherm. Res. 87, 75–93.

Phillips, J.C., Lane, S.J., Lejeune, A.M., Hilton, M., 1995.

Gum rosin–acetone system as an analogue to the degassing behaviour of hydrated magmas. Bull. Volcanol. 57, 263–268.

Proussevitch, A.A., Sahagian, D.L., Kutolin, V.A., 1993. Stability of foams in silicate melts. J. Volcanol. Geotherm. Res. 59, 161–178.

Proussevitch, A.A., Sahagian, D.L., 1996. Dynamics of coupled diffusion and decompressive bubble growth in magmatic systems. J. Geophys. Res. 101, 17447–17455.

Sahagian, D.L., Proussevitch, A.A., 1998. 3D particle size distributions from 2D observations: Stereology for natural applications. J. Volcanol. Geotherm. Res. 84, 173–196.

Sarda, P., Graham, D., 1990. Mid-ocean ridge popping rocks: implications for degassing at ridge crests. Earth Planet. Sci. Lett. 97, 268–289.

Scriven, L.E., 1959. On the dynamics of phase growth. Chem. Eng. Sci. 10, 1–13.

Simakin, A.G., Salova, T.P., 2001. Evolution of bubble size distribution during the gradual degassing of granitic melt. Experiment. Data Geochem. Int. 39, 258–267.

Simakin, A.G., Armienti, P., Epel'baum, M.B., 1999. Coupled degassing and crystallization: Experimental study at continuous pressure drop, with application to volcanic bombs. Bull. Volcanol. 61, 275–287.

Sparks, R.S.J., 1978. The dynamics of bubble formation and growth in magmas: A review and analysis. J. Volcanol. Geotherm. Res. 3, 1–37.

Sparks, R.S.J., Brazier, S., 1982. New evidence for degassing processes during explosive eruptions. Nature 295, 218–220.

Toramaru, A., 1989. Vesiculation process and bubble size distributions in ascending magmas with constant velocities. J. Geophys. Res. 94, 17523–17542.

Toramaru, A., 1990. Measurement of bubble-size distributions in vesiculated rocks with implications for quantitative estimation of eruption processes. J. Volcanol. Geotherm. Res. 43, 71–90.

Tuckwell, H.C., 1988. Elementary Applications of Probability Theory. Chapman and Hall, 225 pp.

Turcotte, D.L., 1992. Fractals and Chaos in Geology and Geophysics. Cambridge University Press, Cambridge.

Watson, E.B., 1994. Diffusion in volatile-bearing magmas. In: Carroll, M.R., Holloway, J.R. (Eds.), Reviews in Mineralogy, Vol. 30. Mineralogical Society of America, pp. 371–411.

Whitham, A.G., Sparks, R.S.J., 1986. Pumice. Bull. Volcanol. 48, 209–223.

Zhang, Y., Behrens, H., 2000. H_2O diffusion in rhyolitic melts and glasses. Chem. Geology 169, 243–262.